Journal of Alloys and Compounds 509 (2011) 4176–4184

Contents lists available at ScienceDirect

Journal of Alloys and Compounds

journal homepage: www.elsevier.com/locate/jallcom

Mechanochemical solid state synthesis of $(Cd_{0.8}Zn_{0.2})S$ quantum dots: Microstructure and optical characterizations

S. Sain, S.K. Pradhan*

Department of Physics, The University of Burdwan, Golapbag, Burdwan 713104, West Bengal, India

ARTICLE INFO

Article history:
Received 24 November 2010
Received in revised form 3 January 2011
Accepted 4 January 2011
Available online 12 January 2011

Keywords:
Nanostructured materials
Mechanical alloying
X-ray diffraction
Microstructure
TEM
Optical properties

ABSTRACT

$(Cd_{0.8}Zn_{0.2})S$ quantum dots with a mixture of both cubic (Zinc-blende) and hexagonal (Wurtzite) phases have been prepared within 75 min by mechanical alloying the stoichiometric mixture of Cd, Zn and S powders at room temperature in a planetary ball mill under Ar. The Rietveld analysis of X-ray powder diffraction data reveals relative phase abundances of both cubic and hexagonal phases and several microstructure parameters like lattice parameters, particle sizes, lattice strains, concentrations of different kinds of stacking faults, etc. in both the phases. At the time of formation, hexagonal phase dominates over the cubic phase (molar ratio ~0.6:0.4), but in course of milling up to 15 h, the hexagonal phase partially transforms to cubic phase and the molar ratio becomes ~0.4:0.6. Particle sizes of hexagonal and cubic phases reduce to ~4.5 nm and 12.5 nm, respectively, after 15 h of milling. The hexagonal phase contains a significant amount of lattice strain in comparison to cubic phase. The presence of different kinds of stacking faults is revealed clearly from the high resolution transmission electron microscope (HRTEM) images.

1. Introduction

In recent years, there has been considerable interest in synthesis and characterization of II–VI compound chalcogenide semiconductors in nanocrystalline form because of their potential applications in different fields of solid state physics [1]. Among several interesting semiconducting nanocrystals, CdZnS nanocrystals are being widely used as wide band-gap window material in hetero junction solar cells [2–6], photoconductive devices [5], wave guides [7], lasers [8,9] and optical switches [10]. In solar cell systems, the replacement of nanocrystalline CdS with relatively higher band-gap ternary CdZnS results in decrease in window absorption losses and thereby increase in the short circuit current in the solar cell [11]. Biological aspect of semiconductor nanocrystals is to understand the complex spatio–temporal interplay of bio molecules from the cellular to the integrative level, researchers mostly use semiconductor nanocrystals for fluorescent labeling of both *in vivo* cellular imaging and *in vitro* assay detection [12].

The optical properties of quantum dots (QDs) having particle size well below the Bohr exiton radius are defined by their size and surface chemistry and they differ significantly from their bulk properties [13]. The band-gap of ternary $Cd_xZn_{1-x}S$ can be fine tuned by tuning composition 'x' for the optimization of parameters of solar cells and fabrication of new opto-electronic devices.

It has been reported earlier [14,15] that the mechano synthesized QDs contain significant amount of lattice strain and different kinds of lattice imperfections including stacking faults. To understand the changes in different properties of these QDs it is therefore, essential to characterize their microstructure in terms of several lattice imperfections generated in these QDs. In most of the earlier cases, changes in properties of QDs were believed to be solely from size confinement effect. Because of size confinement of QDs, there is a reasonable probability of presence of lattice imperfections in these QDs, which was somehow ignored, overlooked or not properly assessed in most of the earlier work. But, we feel, it needs to explore their microstructure in detail for a better understanding and proper interpretation of significant changes in different properties of QDs.

It is now well established that the bulk CdZnS can exist in both hexagonal (43598-ICSD, Sp. Gr. $P6_3mc$ $a = 3.95$ Å, $c = 6.42$ Å) and cubic phases (620389-ICSD, Sp. Gr. F-43m, $a = 5.434$ Å). Nanocrystalline CdZnS may also take both structures of bulk CdZnS. Like ZnS and CdS, the cubic phase of CdZnS is more stable in nanocrystals [14,15]. It may be noted that most intense reflections of both cubic and hexagonal phases appear almost at the same 2θ positions in the XRD pattern. Particularly, in case of QDs these peaks

* Corresponding author. Tel.: +91 342 2657800; fax: +91 342 2657800.
E-mail address: skp_bu@yahoo.com (S.K. Pradhan).

0925-8388/$ – see front matter © 2011 Elsevier B.V. All rights reserved.
doi:10.1016/j.jallcom.2011.01.035

are very broad and as a result, they appear to be completely overlapped. If the presence of any of these phases is nominal, it is almost impossible to detect that phase, either from transmission electron microscopy (TEM) or by any ordinary X-ray diffraction analysis. However, the presence as well as the quantitative phase estimation of the nominal phase can be made in a precise way by considering all its reflections by structure and microstructure refinement methodology, such as the Rietveld method [14–22].

Semiconductor nanocrystals were prepared by several chemical and physical methods [23–29]. Dutkova et al. [30] synthesized nanocrystalline $Cd_xZn_{1-x}S$ by mechanochemical route from corresponding acetates. But, so far, there is no report on single step synthesis of CdZnS by mechanical alloying (MA) the elemental Cd, Zn and S powders at room temperature and its microstructure characterization in terms of lattice imperfections. Reduced particle size and heavy plastic deformation produced in MA introduce a high density of lattice imperfections in ball milled powders which in turn results in peak-broadening of their X-ray powder diffraction profiles [14]. In addition to this, shift in peak-positions and asymmetry in peak shape with respect to the XRD pattern of bulk counter part can also be observed in presence of different kinds of stacking faults, small particle size, lattice strain, change in lattice parameters, residual stress, etc. [31].

In the present study, CdZnS QDs are synthesized by MA the elemental Cd, Zn and S powders milled under Ar in a high energy planetary ball mill for different durations. The synthesis mechanism is observed through successive structural changes in XRD patterns of ball milled powders. Microstructure of these powders is characterized by refining their XRD patterns in terms of several lattice imperfections like stacking faults probabilities of different kinds, particle size, lattice strain, change in lattice parameters and relative phase abundances of cubic and hexagonal phases. Structural and micro/nano structure features are also revealed from high resolution transmission electron microscopy (HRTEM) images, which agree quite well with X-ray measurements. The main objectives of this work are to (i) synthesis CdZnS QDs from its elementary constituents in a single step, (ii) investigate the synthesis mechanism of CdZnS QDs by MA, (iii) quantitative estimations of both cubic and hexagonal CdZnS QDs prepared by MA and (iv) quantification of lattice imperfections present both in cubic and hexagonal CdZnS QDs to interpret changes in properties of CdZnS QDs with a proper justification which are not investigated in earlier works on CdZnS QDs [32–39].

2. Experimental procedure

Pure cadmium (purity 99.5%, Sigma–Aldrich), zinc (purity 99.5%, Loba Chem.) and sulfur powders (purity 99.5%, Merck) taken, respectively, in (0.4:0.1):0.5 molar ratio were used as precursor materials. MA was carried out at room temperature under Ar atmosphere using planetary ball mill (Model P5, M/S Fritsch, GmbH, Germany). Powders were accurately weighed under Ar in a hardened chrome–steel vial of 80 ml volume containing 30 chrome–steel balls kept inside the glove bag and the vial was sealed properly under flowing Ar. The sealed vial containing powders and balls was then mounted on the rotating disk of ball mill. Powders were milled for a particular time and a part of the milled sample was taken out from the vial under Ar for X-ray measurement. The progress of milling was interrupted at different interval of time and the change in X-ray powder diffraction patterns of ball-milled samples was noticed.

The X-ray powder diffraction profiles of the unmilled mixture and all ball milled samples were recorded using Ni-filtered CuKα radiation from a highly stabilized and automated Philips X-ray generator (PW 1830) operated at 40 kV and 20 mA. The step-scan data (of step size 0.05° 2θ and counting time 5–10 s depending on the peak intensity) were recorded for the entire angular range 20° to 80° 2θ. Microstructures as well as selected area electron diffraction (SAED) patterns of the ball milled samples were revealed by using high resolution transmission electron microscope (HRTEM) (JEOL JEM 2100) equipped with GATAN CCD camera. All samples were dispersed in ethanol, sonicated for a long time and subsequently, a drop of it was put on a carbon coated copper grid for TEM study. The optical absorption spectra of all ball milled samples were obtained from Shimadzu UV–vis spectrometer (Shimadzu UV-1800) in the wavelength range 200–800 nm.

3. Method of analysis

In the present study, we have adopted the Rietveld's powder structure refinement analysis [16–21] of X-ray powder diffraction data to obtain the refined structural parameters, such as atomic coordinates, occupancies, lattice parameters, thermal parameters, etc. and microstructure parameters such as particle size, r.m.s. lattice strain and stacking faults. The Rietveld's software MAUD 2.26 [20] specially designed to refine simultaneously both the structural and microstructure parameters through a least-square method. The peak shape is assumed to be a pseudo-Voigt (pV) function with asymmetry because it takes individual care for both the particle size and strain broadening of the experimental profiles. The background of each pattern is fitted by a polynomial function of degree 4. The theoretical X-ray powder diffraction pattern is simulated containing all these five Cd, Zn, S, cubic CdZnS and hexagonal CdZnS phases in a single pattern as the patterns are composed of reflections from these phases. The Marquardt least-squares procedure is adopted for minimization of the difference between the observed and simulated powder diffraction patterns and the minimization is monitored using the reliability index parameter, R_{wp} (weighted residual error), and R_{exp} (expected error). This leads to the value of goodness of fit (GoF) [16–21]:

$$\mathrm{GoF} = \frac{R_{wp}}{R_{exp}}$$

The peak-broadening, peak-asymmetry and peak-shift of the experimental profiles are fitted by refining the particle size, lattice strain values, lattice parameters (including zero-shift error) and stacking fault parameters. Refinements of all parameters are continued till convergence is reached with the value of the quality factor, GoF very close to 1 (varies between 1.1 and 1.3), which confirms the goodness of refinement. It may be noted that the Cagliotti parameters U, V and W [19], instrumental asymmetry and Gaussianity parameters [20] are obtained for the instrumental setup (instrumental corrections) using a Si standard and kept fixed during refinements.

4. Results and discussion

4.1. Microstructure characterization by XRD and HRTEM

All X-ray powder diffraction patterns of stoichiometric mixture of Cd, Zn and S powders prepared at different milling times are shown in Fig. 1. It clearly shows that the unmilled (0 h) mixture is consisted of elemental compositions, i.e. cadmium (JCPDF #05-0674, hexagonal, Sp. Gr. P63/mmc a = 2.9793 Å, c = 5.6181 Å), zinc (JCPDF #04-0831; hexagonal, Sp. Gr. P63/mmc, a = 2.665 Å, c = 4.947 Å) and sulfur (ICSD file # 412326, Sp. Gr. Fddd, orthorhombic, a = 10.393 Å; b = 12.762 Å; c = 24.436 Å) phases. All these reflections are well resolved and at higher scattering angle split clearly into Cu $K_{\alpha 1-\alpha 2}$ doublets. It indicates that particle sizes of starting ingredients are quite large and they are almost free from lattice strain. It may be noted that except these reflections there are some weak reflections in the pattern. These reflections are identified as from the CdO (JCPDF #05-0640, cubic, Sp. Gr. Fm3m, a = 4.6953 Å) phase which is formed in unmilled sample during XRD data collection under open air.

It is found that just after 75 min of milling, ternary $Cd_{0.8}Zn_{0.2}S$ phase is formed through an exothermic reaction (followed by a mild explosion) among the elemental powders inside the vial and all reflections of CdZnS phase appear clearly in the XRD pattern. This kind of mild explosion in formation of ZnS and CdS phases was already noticed in our previous work [14,15]. These reflections are identified as from both cubic and hexagonal phases and the

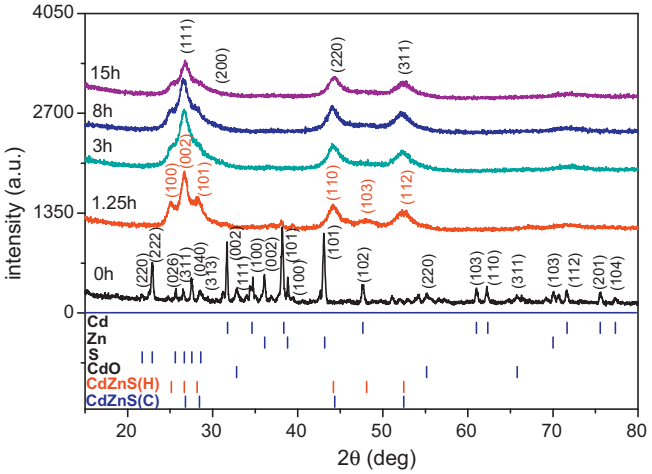

Fig. 1. X-ray powder diffraction patterns of unmilled and ball milled Cd, Zn and S powders (Cd:Zn = 80:20 mol) milled for different durations. CdZnS(C) denotes the cubic and CdZnS(H) represents the hexagonal phase.

hexagonal phase is found to have the major contribution. There is a small amount (~0.9%) of the elemental Cd powder traced in the XRD pattern of the sample. It indicates that the prepared CdZnS phase is almost stoichiometric in composition. As there is no reflection from milling media in the ball milled XRD patterns, it has been confirmed that these powders are free from contamination of milling media, or the level of contamination is below the detectable range (<1 wt%). As well as there is no oxide reflection of constituent elemental powders, so the contamination from atmosphere of milling can be ruled out.

Dutkova et al. [30] noticed a phase transition from hawleyite (cubic CdS: Sp. Gr. F-43m) to sphalerite (cubic ZnS: Sp. Gr. F-43m) in $Cd_{0.5}Zn_{0.5}S$ with increasing Zn content. The apparently isolated reflection at $2\theta \sim 26.7^\circ$ in between (1 0 0) and (1 0 1) reflections of hexagonal phase, is the position of both cubic (C) (1 1 1) and hexagonal (H) (0 0 2) phases and appears as the major intense reflection in XRD pattern due to overlapping of both CdZnS(C) (1 1 1) and CdZnS(H) (0 0 2) reflections (Fig. 2(a)). This kind of complete peak overlapping is also observed at $2\theta \sim 44^\circ$ and $2\theta \sim 52.4^\circ$ with overlapping CdZnS(C) (2 2 0)/CdS(H)(1 1 0) and CdZnS(C) (3 1 1)/CdZnS(H) (1 1 2) reflections, respectively. Due to small particle size, peaks are broadened and thereby partially or completely overlapped and it is therefore very difficult to find any individual reflection of minor cubic phase in the XRD patterns of these ball milled samples. Initially, XRD patterns of all milled powders are appeared to be from a single hexagonal phase and in the course of milling it transforms slowly to cubic phase. However, a critical comparison of intensities of individual reflections of both hexagonal and cubic phases clearly reveals the presence of a minor cubic phase (Fig. 2(a)). To the best of our knowledge, so far, there is no report on simultaneous presence of hexagonal and cubic phases in ternary CdZnS phase. Patidar et al. [32], and Kumar et al. [33] prepared single phase hexagonal CdZnS thin films by vacuum evaporation method. Dzhafarov et al. [34] synthesized the hexagonal CdZnS thin films by Zn diffusion in CdS lattice. Akyuz et al. [35] reported the formation of $Zn_{1-x}Cd_xS$ films using ultrasonic spray pyrolysis, but the X-ray diffraction pattern of the film consists of reflections from all hexagonal CdZnS, CdS and ZnS phases. Chavhan et al. [36] synthesized the $Cd_{1-x}Zn_xS$ thin film grown on an ITO substrate using a chemical bath deposition technique and the annealed films posses a crystalline nature with a hexagonal structure. Rafea et al. [37] prepared the stoichiometric cubic $Cd_{0.5}Zn_{0.5}S$ phase by dip coating method onto glass substrate. Raviprakash et al. [38] and Li et al. [39] obtained the hexagonal (wurtzite) CdZnS phase by chemical spray pyrolysis and chemical reaction, respectively. In most of the above cases, the hexagonal phase was found to be present as a single phase. However, it is really difficult to trace out the presence of minor cubic phase in the XRD pattern and it is more difficult, if not possible, to obtain the content of the cubic phase where there is no individual reflection of the phase and all major reflections are severely overlapped with hexagonal reflections. This can only be done when the XRD pattern is analyzed very carefully by the whole profile fitting technique based on structure and microstructure refinements, like the Rietveld method of structure and microstructure refinement. But, in none of the previous reports, the Rietveld method was adopted. The phase identification was done from the JCPDS files and crystallite/particle size was obtained from the simplified Scherrer equation, in which the peak broadening was considered solely due to small particle size. In some cases, particle size was estimated from peak broadening considering only some selected reflections and in others, there was no report on the 'instrumental broadening' correction for estimation of particle size by Scherrer equation. It may be noted that, XRD patterns of ball milled samples shown in Fig. 1 seems to belong to a single hexagonal phase, and the presence of cubic phase may be overlooked or ignored easily if we do not critically compare the intensities of individual reflections of hexagonal phase. In the presence of minor cubic phase, the Scherrer method is not adequate to analyze this kind of complicated XRD pattern with several overlapping reflections from both of the phases.

It is well established that properties of a crystalline material are directly related to its structure and microstructure. There are several methods for characterization of crystal structure but for microstructure characterization in terms of lattice imperfections of different kinds inside a small crystallite like QDs is very few. In the present case we have adopted the Rietveld method of structure and microstructure refinements as this is the best method for microstructure characterization for materials having significant number of overlapping reflections in XRD pattern due to the influence of lattice imperfections like stacking faults, changes in lattice parameter, small particle size, lattice strain, etc. This method is able to estimate quantitatively all these lattice imperfections as well as relative phase abundances in a material containing more than one phase. In the present study, the simulated XRD patterns for Rietveld analysis are generated with the following phases: (i) Cd, (ii) Zn, (iii) S, (iv) CdZnS (hexagonal; ICSD file #43598) and (v) CdZnS (cubic; ICSD file #620389). All experimental XRD patterns of unmilled and all ball-milled samples are fitted very well by refining the structural and microstructure parameters of respective simulated patterns (Fig. 2(b)). The GoF in all cases lies in between 1.1 and 1.3 which signifies that the fitting qualities are good enough for all experimental patterns. The residual of fittings ($I_0 - I_C$) in between observed (I_0) and calculated (I_C) intensities of each fitting are plotted below the respective patterns. Peak positions of all reflections of all five phases are marked (|) and shown at the bottom of the plot. It is evident clearly from the plot that both hexagonal and cubic CdZnS phases are formed after just 75 min of milling and a small amount of Cd (~0.9%) powder remains unreacted.

The Rietveld analysis of XRD patterns clearly reveals the presence of cubic CdZnS phase. The simultaneous presence of both hexagonal and cubic CdZnS phases and the transformation of the hexagonal phase to cubic phase with increasing milling time are clearly shown in Fig. 2(c) and (d). The contribution of cubic phase is relatively small at the beginning and all its reflections are significantly broad and as a result, severely overlapped with hexagonal reflections. It is therefore, very difficult to notice its presence even by HRTEM. The analysis also reveals the presence of both hexagonal and cubic phases in all ball milled samples up to 15 h, in different proportions. The indexed selected area electron diffraction (SAED) pattern of 15 h ball milled powder is shown in Fig. 3. It may be

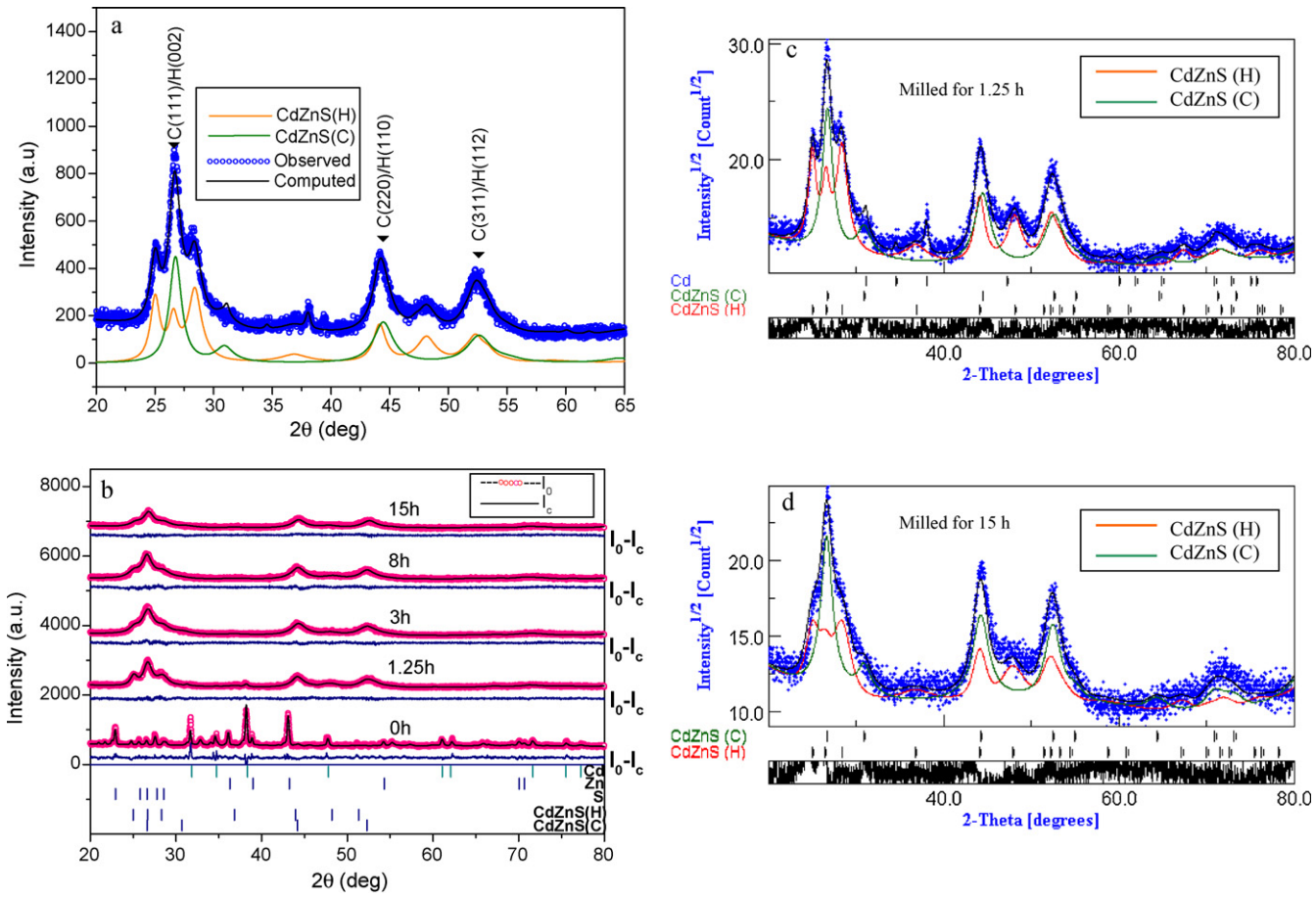

Fig. 2. (a) Highly overlapped hexagonal and cubic reflections of ball milled prepared $Cd_{0.8}Zn_{0.2}S$ phase. All three major peaks are strongly overlapped, (b) observed (o) and calculated (−). X-ray powder diffraction patterns of unmilled and ball-milled samples of Cd, Zn and S (Cd:Zn = 80:20 molar ratio) powders milled for different durations revealed from the Rietveld powder structure refinement analysis, (c) variation of cubic and hexagonal phases in 1.25 h milled sample and (d) that for 15 h milled sample from the Rietveld analysis: increase in cubic phase and decrease in hexagonal phase is clearly noticed with increase in milling time.

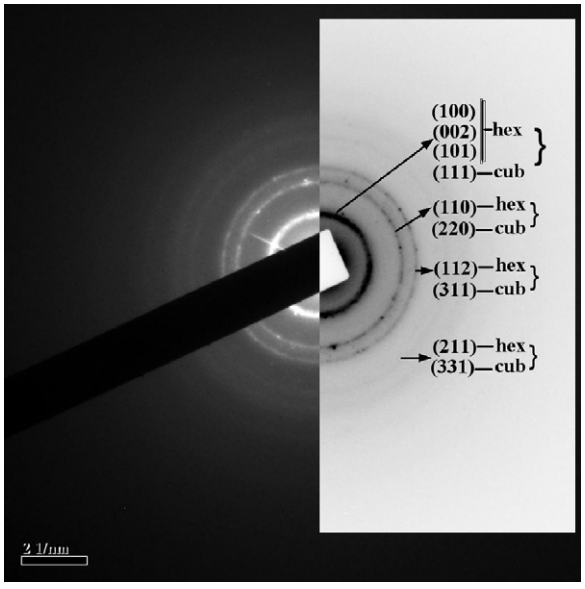

Fig. 3. Selected area electron diffraction (SAED) image of 15 h ball milled $Cd_{0.8}Zn_{0.2}S$ QDs shows high degree of overlapped rings of the cubic and hexagonal phases.

noted that the diffraction lines have been indexed in accordance to the corresponding XRD pattern, because owing to shorter wavelength of electron beam, first four reflections from hexagonal and cubic phases are entirely overlapped into a single Debye–Scherrer ring in the SAED pattern. It seems that the ring belongs to a single cubic phase and it is hardly matter to show the presence of minor hexagonal phase in the SAED pattern. It indicates that X-ray analysis employing the Rietveld refinement is a superior method for identification of a minor phase having severely overlapping reflections. Another very important feature in the XRD patterns of nanocrystalline materials is the shift in peak positions which was sometimes overlooked or considered only due to change in lattice parameters in earlier studies [32,34]. However, the shift in peak positions of nanomaterial in comparison to its bulk counterpart is caused due to (i) presence of stacking faults, (ii) change in lattice parameters and (iii) long-range residual stress in nanomaterials [31]. Sometimes, this shift is so small that it may be overlooked if the XRD patterns are not analyzed by structure and microstructure refinements simultaneously. In the present study, the adopted software MAUD 2.26 [20] provides both structural and microstructure analyses based on the X-ray line profile analysis methodology of Warren [40] and accounts for quantitative estimations of all these microstructure parameters causing peak shift. As the particle sizes of both phases are very small, the existence as well as the contribution of residual stress in peak-shift may be neglected. Considering the resultant peak-shift in ball milled samples is due to both the

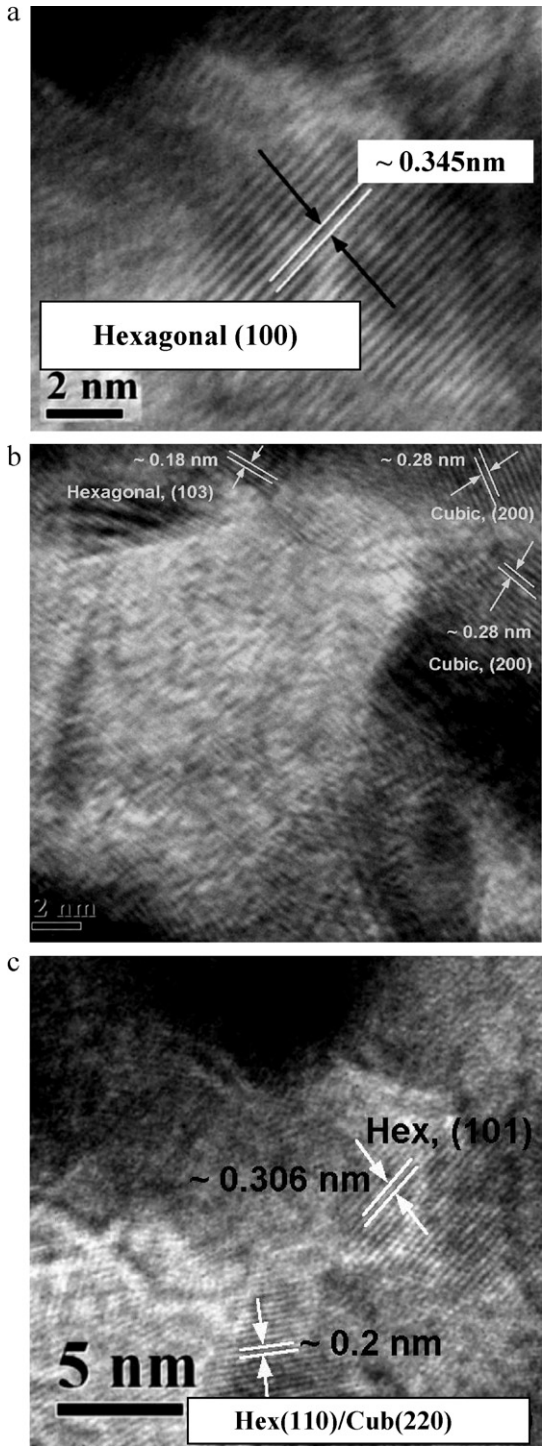

Fig. 4. (a) Inter planar distance, d_{100} of hexagonal (1 0 0) plane. (b) Presence of both hexagonal and cubic planes in 15 h milled sample. (c) Presence of both hexagonal and cubic planes in 15 h milled sample.

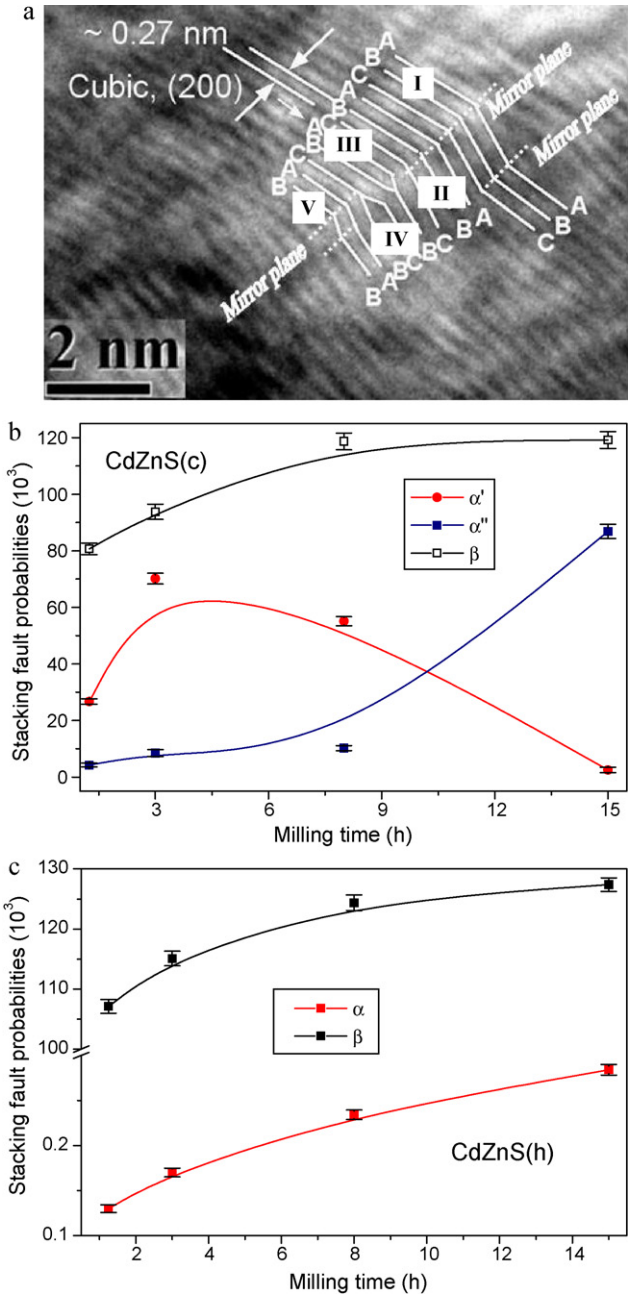

Fig. 5. (a) HRTEM lattice image of cubic $Cd_{0.8}Zn_{0.2}S$ QDs milled for 15 h showing the presence of intrinsic (α'), extrinsic (α'') and twin faults (β) in the stacking sequence of (2 0 0) planes of cubic QDs. (b) Variations of different kinds of stacking fault probabilities with increasing milling time per 1000 atomic layers in cubic $Cd_{0.8}Zn_{0.2}S$. (c) Variations of different kinds of stacking fault probabilities with increasing milling time per 1000 atomic layers in hexagonal phase of $Cd_{0.8}Zn_{0.2}S$.

change in lattice parameter and stacking fault probabilities of different nature (intrinsic and extrinsic stacking faults, twin faults), the profile fitting quality improves significantly and the concentrations of different kinds of stacking faults in ball milled samples are obtained from the Rietveld analysis.

The presence of different lattice planes of both cubic and hexagonal phases are identified in the HRTEM images of the 15 h ball milled sample and shown in Fig. 4(a)–(c). The measured values of the hexagonal d_{100}, d_{101}, d_{103} and cubic d_{200} are ~3.45 Å, 3.06 Å, 1.8 Å and 2.8 Å, respectively, and are very close to their respective reported values as obtained from respective ICSD entries. The inter planar distances of hexagonal d_{110} and cubic d_{220} lie in close proximity of ~2 Å. So, in Fig. 4(c) the observed lattice fringes are either from hexagonal d_{110} or from cubic d_{220} or perfectly superimposed between these lattice planes. It is evident from Figs. (2a) and 4(a)–(c) that inter planar distances of hexagonal (0 0 2), (1 1 0) and (1 1 2) planes are almost similar to those of cubic (1 1 1), (2 2 0) and (3 1 1) planes, respectively, which signifies a phase relationship between these two phases. The presence of different kinds of stacking faults is clearly evidenced in the HRTEM image of 15 h (Fig. 5(a)) milled sample. The atomic layers shown

in these images are identified as (2 0 0) plane of cubic CdZnS phase with inter planar spacing ~2.70 Å. A careful observation in Fig. 5(a) clearly reveals the presence of intrinsic (α'), extrinsic (α'') and twin faults (β). In zones-I and V, the normal stacking sequence of atomic planes has been mirror imaged two times and multiple twin faults have been generated in these regions. In zone-II, a single twin fault is generated as the normal stacking sequence has been mirror imaged once in this region. In zone-III, two successive atomic planes have been merged into a single plane, which signifies the missing of an atomic plane from the normal stacking sequence and thereby an intrinsic stacking fault is generated in this region. The reverse effect has been observed in zone-IV where a single atomic plane splits into two similar atomic planes. This is similar to inclusion of an extra atomic plane into the normal stacking sequence and thereby an extrinsic stacking fault is generated in this region. It may be noted that there are similar other regions of stacking faults in this high resolution electron micrograph. Though the HRTEM image confirms the presence of different kinds of stacking faults but their concentrations cannot be measured from this extremely localized image. The concentration of stacking faults in terms of probability of stacking faults in among 10^3 atomic layers have been worked out employing the peak shift analysis as suggested by Warren [40] and adopted in the Rietveld software MAUD 2.26 [20]. This analysis reveals that all intrinsic (α') nature of stacking faults (missing planes) in cubic phase are generated initially (~27 atomic planes are missing from 1000 layers of stacking) with a significant amount (~80 times in 1000 atomic planes) of twin faults (β). In the progress of milling, the probability of α' increases up to 3 h of milling and then decreases continuously up to 15 h of milling where only ~3 atomic planes are found to be absent among 1000. In the same time interval, probability of β increases slowly up to ~120 times among 1000 planes. The probability of extrinsic stacking fault (α'') increases continuously from inclusion of ~5–85 planes per 1000 planes. The variation of these stacking faults is depicted in Fig. 5(b). This trend of variation of stacking fault probabilities may be explained in the following way: (i) initially, atomic planes are slipped from the normal stacking sequence and intrinsic stacking faults are created. With increasing milling duration, the probability of slip decreases sharply, and (ii) later on, these slipped planes start to insert into normal stacking sequence and extrinsic stacking faults are created at the higher time of milling. The deformation stacking fault (α) and twin/growth fault (β) probabilities of the hexagonal phase has also been worked out from peak broadening analysis in the same manner. It is evident from Fig. 5(c) that the generation of probabilities of both α and β in hexagonal phase increases continuously with increasing milling time. However, the probability of deformation fault, α in hexagonal phase is quite low in comparison to the growth fault, β as well as the stacking faults in cubic phase. The probability of growth faults in hexagonal phase is very close to the twin faults obtained for cubic phase. It seems that both cubic and hexagonal phases are highly deformed by twin type of stacking faults.

The relative phase abundances of different phases in unmilled and all ball-milled samples are obtained from Rietveld analysis and are shown in Fig. 6. It may be noted that, initially, the phase content of sulfur is more than 0.80 mol fraction in the unmilled sample and with increasing milling time, the mixture of Cd, Zn and S powder is supposed to become homogeneous and stoichiometric in composition (Cd: Zn~0.8:0.2 mol fraction) and formation of $Cd_{0.8}Zn_{0.2}S$ phase starts after 75 min of milling (shown as dotted lines). However, the apparent higher composition of sulfur phase may be attributed to the lubricating nature of the sulfur powder. It covers almost the entire surface of the unmilled sample during sample loading into XRD sample holder through pressing and smoothing the surface to reduce sample surface roughness. We have also noticed the same phenomena during the preparation of

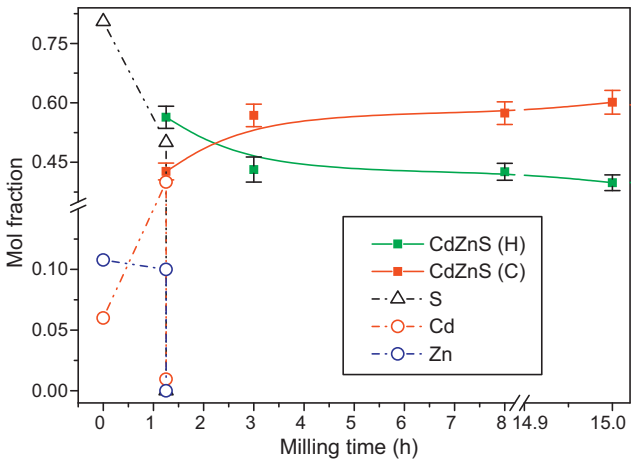

Fig. 6. Variations of phase contents (mol fraction) of different phases in unmilled and ball milled mixture of Cd, Zn and S (Cd;Zn = 80:20 mol) with increasing milling time. Initial variation (supposed to be) of mol fraction elemental Cd, Zn and S powders are shown as dotted lines.

ZnS and CdS [14,15]. It is interesting to note that whenever the mixture becomes stoichiometric in composition after 75 min of milling, both the hexagonal and cubic $Cd_{0.8}Zn_{0.2}S$ phases are formed simultaneously with hexagonal phase as the major phase. In the course of milling, content of hexagonal phase decreases gradually and that of cubic phase increases continuously, up to 15 h of milling. As there is a phasal relationship between these two phases, such as $(0\,0\,2)_{hex} \,||\, (1\,1\,1)_{cub}$, this kind of polymorphic phase transformation may be observed in ball mill processing. It is well established that the cubic phase is more stable in $Cd_{0.8}Zn_{0.2}S$ QDs than the hexagonal phase, a longer milling time may lead to achieve a completely cubic phase. As the phase conversion rate is very slow, single phase QDs with this composition may not be synthesised by the present process of ball milling.

The changes in lattice parameters of both cubic and hexagonal phases in ball-milled samples are shown in Fig. 7. It is evident from the plot that the lattice parameters of all phases remain almost invariant with increasing milling time.

Particle sizes of both cubic and hexagonal phases reduce very rapidly at the initial stage of milling and their variations with increasing milling time are shown in Fig. 8(a). Particle size of cubic phase reduces gradually from ~42 nm to ~29 nm within 8 h of milling, and then decreases to ~12 nm after 15 h of milling. The

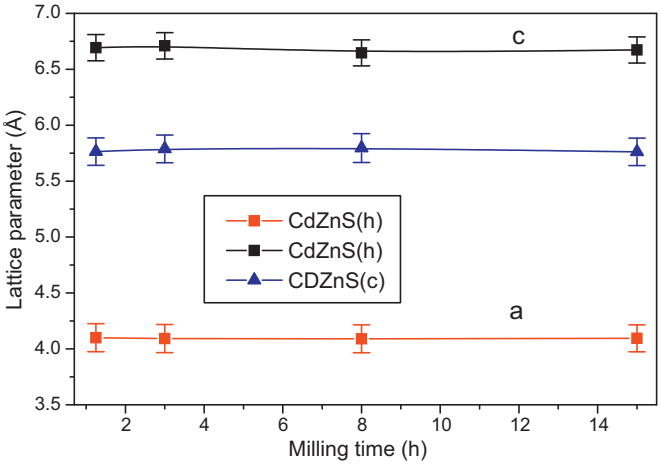

Fig. 7. Variation of lattice parameters of both cubic and hexagonal phases of $Cd_{0.8}Zn_{0.2}S$ QDs with increasing milling time.

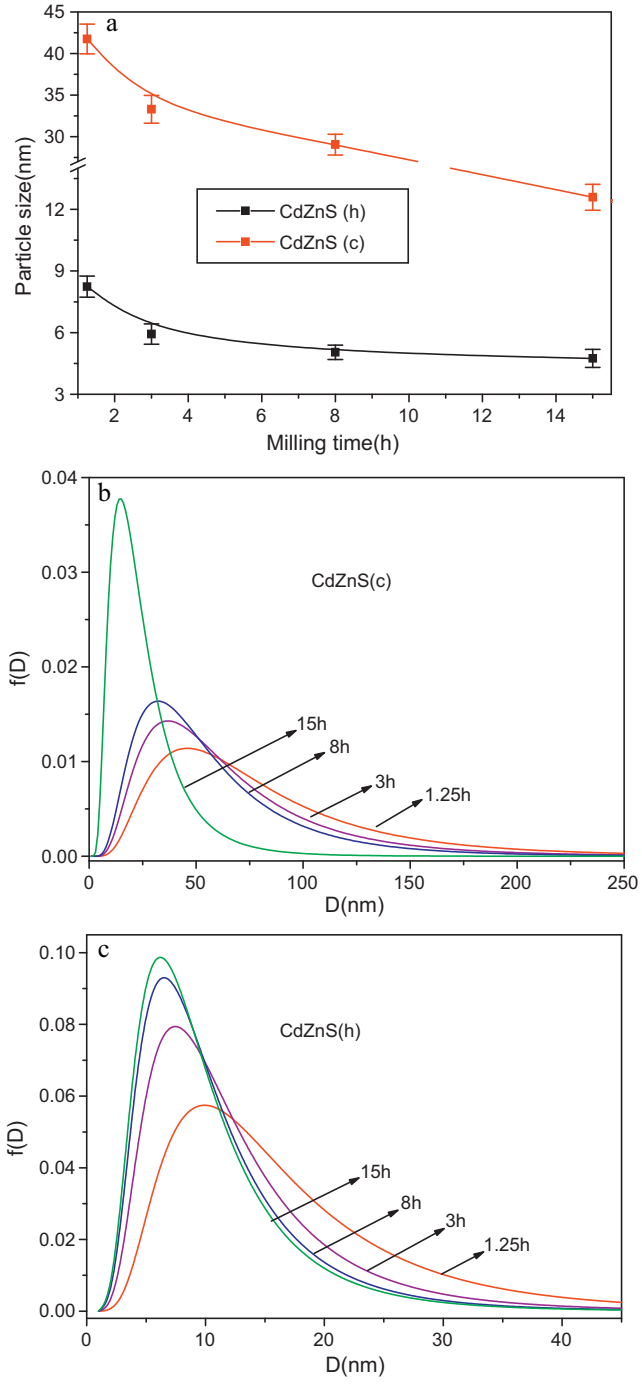

Fig. 8. (a) Variation of particle sizes of both cubic and hexagonal phases of $Cd_{0.8}Zn_{0.2}S$ with increasing milling time. (b) Distributions of grain diameter (particle size) of cubic $Cd_{0.8}Zn_{0.2}S$ QDs in ball milled mixture of Cd, Zn and S(Cd:Zn = 80:20 mol) at different milling time showing mono dispersed nature with increasing milling hours. (c) Distributions of grain diameter (particle size) of hexagonal $Cd_{0.8}Zn_{0.2}S$ QDs in ball milled mixture of Cd, Zn and S (Cd:Zn = 80:20 mol) at different milling time showing mono dispersed nature with increasing milling hours.

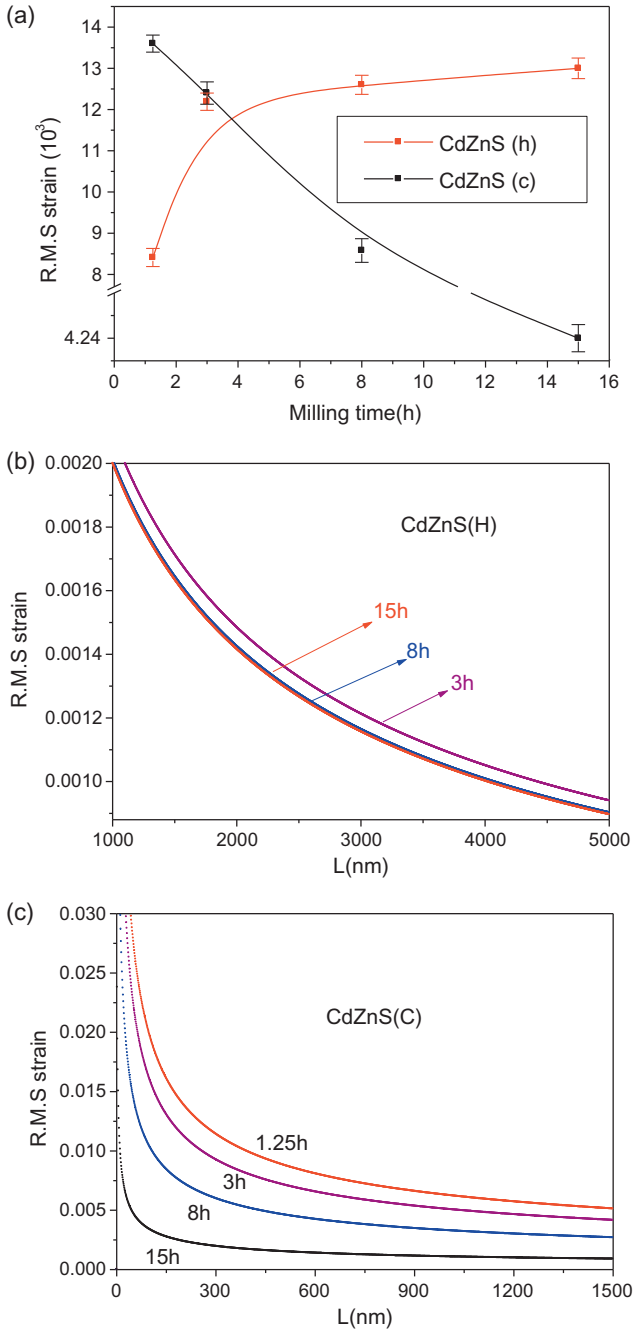

Fig. 9. (a) Variations of r.m.s lattice strain of both cubic and hexagonal phases of $Cd_{0.8}Zn_{0.2}S$ QDs with increasing milling time. (b) Distributions of r.m.s. strains of hexagonal CdZnS QDs in ball milled mixture of Cd, Zn and S (Cd:Zn = 80:20 mol) at different milling time. ($L = na_3$, n = harmonic number, a_3 = lattice parameter). (c) Distributions of r.m.s. strains of cubic CdZnS QDs in ball milled mixture of Cd, Zn and S (Cd:Zn = 80:20 mol) at different milling time. ($L = na_3$, n = harmonic number, a_3 = lattice parameter).

hexagonal phase is formed with ~8 nm particle size and reduces rapidly to ~5.9 nm within 3 h of milling, and then very slowly to ~4.5 nm after 15 h of milling. In both the cases, particles are found to be isotropic in nature. The particle size distributions for both cubic and hexagonal phases revealed from the Rietveld analysis are shown in Fig. 8(b) and (c), respectively. It is interesting to note that with increasing milling time the size as well as the range of distribution reduces simultaneously. After 15 h of milling, the most probable value of particle size becomes ~13 nm in case of the cubic phase and ~5.5 nm in case of hexagonal phase. In 15 h ball-milled sample, the particle size distribution becomes almost monodispersed. It indicates that monodispersed cubic and hexagonal CdZnS QDs can be prepared by this top–down method.

The r.m.s. lattice strains generated in both hexagonal and cubic phases during the milling have been obtained from the Rietveld analysis and are shown in Fig. 9(a). It is evident from the variation that the hexagonal phase is formed with relatively small amount of lattice strain. In the course of milling, lattice strain increases

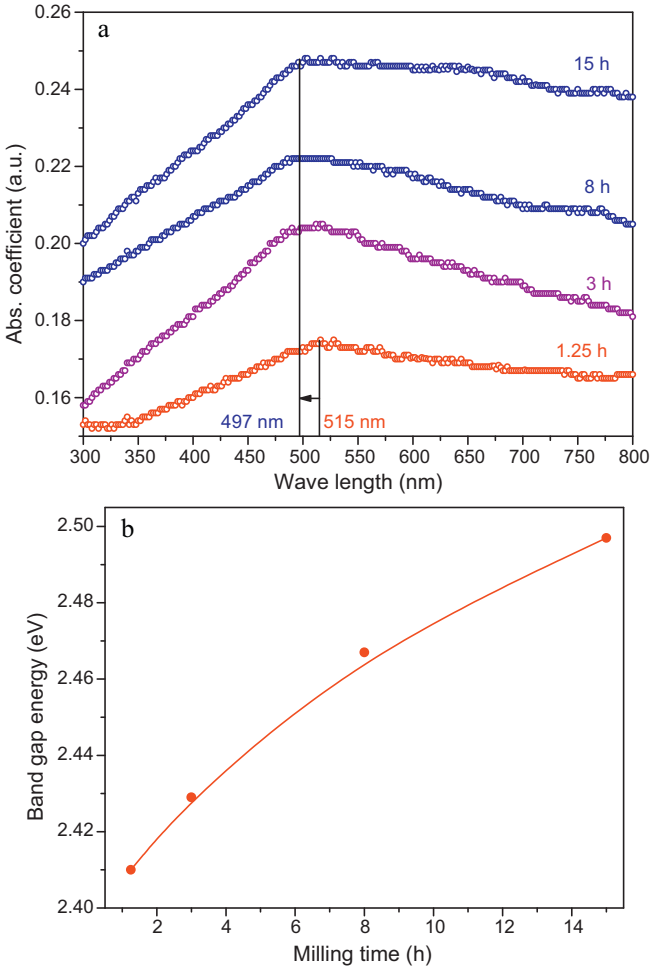

Fig. 10. (a) UV–vis absorption spectra of $Cd_{0.8}Zn_{0.2}S$ powders dispersed in ethanol with different hours of ball milling. (b) Variations of band gap energies (eV) with increasing milling time.

rapidly up to 3 h of milling and then remains almost invariant up to 15 h of milling. However, the cubic phase is formed with relatively higher value of lattice strain which decreases rapidly with increasing milling time. The distributions of lattice strain inside the hexagonal and cubic particle are shown in Fig. 9(b) and (c) respectively. As the particle size reduces with milling time, the length available for strain distribution is also reduced, which is evident in the distribution plot. In both phases, the distribution of lattice strain approaches continuously toward lower value.

4.2. Optical characterization by UV–vis spectrometer

The optical absorption spectra of all these ball milled samples are obtained in the wavelength range 200–800 nm, depicted in Fig. 10(a). The coefficient of absorption of these samples is expected to depend on several factors, such as, surface roughness, dispersion effect, etc. The low value of absorbance in case of $Cd_{0.8}Zn_{0.2}S$ QDs may be due to light scattering at the rough surface of the particles. In the absorption spectra the maximum absorption for sample milled for 75 min appears at 515 nm and that for 15 h milled sample at 497 nm. It indicates that the absorbance edges are in visible region and shift toward shorter wavelength region, i.e. a significant blue-shift is clearly observed with decreasing size of $Cd_{0.8}Zn_{0.2}S$ particles. The optical band gap energy of all these samples are calculated using the Tauc [41] formula applicable for direct band gap semiconductors and plotted in Fig. 10(b). It is evident from the variation that the optical band gap energy of ball milled samples increases continuously with increasing milling time. Both the observed blue shift of absorption edge and the absorption peaks can be attributed to the reduction in particle size, i.e. the quantum confinement effect. The change in kinetic energy due to the reduction in particle size increases the band gap and the energy separation of allowed transitions near the absorbance edge. The latter is mostly responsible for shift in absorption peak position. Again, the appearance of the obvious UV–vis absorption peak is a sign that the as-prepared $Cd_{0.8}Zn_{0.2}S$ nanoparticles are nearly monodispersed which agrees well with already revealed monodispersity of particles from the Rietveld analysis.

Such a blue-shift of the absorption peak for ball-milled $Cd_{0.8}Zn_{0.2}S$ nanoparticles to the UV–vis wavelength range is that only small dispersed particles can float in the solution because floating force merely arises from the solution. The other possibility is that the clean surface of the ball milled $Cd_{0.8}Zn_{0.2}S$ nanoparticles excludes the influence from the interaction or charge transfer between the particle surface and the organic ligand. This means that ball milled samples can reveal the intrinsic optical properties of these nanoparticles without the influence of the capping organic ligand on the particle surface. So, the optical absorbance peaks of these ball milled nanocrystals, which are located within the UV–vis wavelength range, may correspond to the intrinsic band gap energies of the $Cd_{0.8}Zn_{0.2}S$ nanoparticles. It is thus possible to have tune ability on the opto-electronic properties of CdZnS nanoparticles by only varying the particle size for an extensive use.

5. Conclusions

These above observations clearly reveal the following facts about the $Cd_{0.8}Zn_{0.2}S$ QDs synthesized by mechanical alloying of elemental powder precursors:

(1) $Cd_{0.8}Zn_{0.2}S$ QDs with hexagonal and cubic phases have been prepared by top–down physical method of processing for the first time within 75 min of ball-milling the stoichiometric mixture of elemental Cd, Zn and S powders under Ar at room temperature.
(2) Detail microstructure characterization of ball milled $Cd_{0.8}Zn_{0.2}S$ powders by the Rietveld method of structure refinement reveals that the major hexagonal phase is formed initially and the minor cubic phase is formed coherently on the hexagonal lattice.
(3) In the course of milling, the hexagonal phase slowly transforms to cubic phase and after 15 h of milling, the molar ratio of cubic and hexagonal phases reaches to ~0.6: 0.4.
(4) The ball-milled QDs contain different kinds of stacking faults and the Rietveld analysis estimates their concentrations. HRTEM images confirm the presence of different kinds of stacking faults in these QDs.
(5) A distinct blue-shift in absorption edge is noticed and the band gap can be fine tuned as per requirements for a particular purpose by varying the size of these QDs which is synchronous with the time of milling.

Acknowledgments

Authors wish to thank the University Grants Commission (UGC) India, for granting DSA-III programme under the thrust area "Condensed Matter Physics including Laser applications" to the Department of Physics, Burdwan University under the financial assistance of which the work has been carried out. One of the authors S. Sain also wishes to thank University Grants Commission

(UGC) for providing research fellowship to carry out the research work.

References

[1] I.O. Oladeji, L. Chow, C.S. Ferekides, V. Viswanathan, Z. Zhao, Sol. Energy Mater. Sol. Cells 61 (2000) 203–211.
[2] K.T.R. Reddy, P.J. Reddy, J. Phys. D: Appl. Phys. 25 (1992) 1345–1348.
[3] H.S. Kim, H.B. Im, J.T. Moon, Thin Solid Films 214 (1992) 207–212.
[4] Y.K. Jun, H.B. Im, J. Electrochem. Soc.: Electrochem. Sci. Technol. 135 (1988) 1658–1661.
[5] B.M. Basol, J. Appl. Phys. 55 (1984) 601–603.
[6] K.W. Mitchell, A.L. Fahrenbruch, R.H. Bube, J. Appl. Phys. 48 (1977) 4365–4371.
[7] X.F. Duan, Y. Hu, R. Agarwal, C.M. Lieber, Nature 421 (2003) 241.
[8] M.H. Huang, S. Mao, H. Feick, H.Q. Yan, Y.Y. Wu, H. Kind, E. Weber, R. Russo, P.D. Yang, Science 292 (2001) 1897–1899.
[9] K. Bando, T. Sawabe, K. Asaka, Y. Masumoto, J. Lumin. 108 (2004) 385–388.
[10] H. Kind, H. Yan, B. Messer, M. Law, P. Yang, Adv. Mater. 14 (2002) 158–160.
[11] T. Yamaguchi, Y. Yamamoto, T. Tanaka, Y. Demizu, A. Yoshida, Thin Solid Films 281–282 (1996) 375–378.
[12] A. Miyawaki, Dev. Cell 4 (2003) 295–305.
[13] A.L. Rogach, Mater. Sci. Eng., B 69 (2000) 435–440.
[14] S. Patra, B. Satpati, S.K. Pradhan, J. Appl. Phys. 106 (2009) 034313–34318.
[15] S. Patra, B. Satpati, S.K. Pradhan, J. Nanosci. Nanotechnol. 11 (2011) 1–10.
[16] L. Lutterotti, P. Scardi, P. Maistrelli, J. Appl. Crystallogr. 25 (1992) 459–462.
[17] H.M. Rietveld, Acta Crystallogr. 22 (1967) 151–152.
[18] H.M. Rietveld, J. Appl. Crystallogr. 2 (1969) 65–71.
[19] R.A. Young, D.B. Willes, J. Appl. Crystallogr. 15 (1982) 430–438.
[20] L. Lutterotti, Maud Version 2.26, 2010, http://www.ing.unitn.it/~maud/ 19.11.2010.
[21] E.J. Mittemeijer, P. Scardi, Diffraction Analysis of the Microstructure of Materials, Springer, Germany, 2004.
[22] S.K. Pradhan, M. Sinha, J. Appl. Crystallogr. 38 (2005) 951–957.
[23] L.E. Brus, Appl. Phys. A: Mater. Sci. Process 53 (1991) 465–474.
[24] A. Henglein, Top Curr. Chem. 143 (1988) 113–180.
[25] Y. Wang, N.J. Herron, Phys. Chem. 95 (1991) 525–532.
[26] M.G. Bawendi, M.L. Steigerwald, L.E. Brus, Annu. Rev. Phys. Chem. 41 (1990) 477–496.
[27] J.E.B. Katari, V.L. Colvin, A.P. Alivisatos, J. Phys. Chem. 98 (1994) 4109–4117.
[28] M.L. Steigerwald, A.P. Alivisatos, J.M. Gibson, T.D. Harris, R. Kortan, A.J. Muller, A.M. Thayer, T.M. Duncan, D.C. Douglass, L.E. Brus, J. Am. Chem. Soc. 110 (1988) 3046–3050.
[29] J.G. Brennan, T. Siegrist, P.J. Carroll, S.M. Stuczynski, L.E. Brus, M.L. Steigerwald, J. Am. Chem. Soc. 111 (1989) 4141–4143.
[30] E. Dutkova, P. Balaz, P. Pourghahramani, A.V. Nguyen, V. Sepelak, A. Feldhoff, J. Kovac, A. Satka, Solid State Ionics 179 (2008) 1242–1245.
[31] C.N.G. Wagner, Local Atomic Arrangements Studied by X-Ray Diffraction, Gordon and Breach, New York, 1966.
[32] D. Patidar, N.S. Saxena, T.P. Sharma, J. Mod. Opt. 55 (2008) 79–88.
[33] P. Kumar, A. Misra, D. Kumar, N. Dhama, T.P. Sharma, P.N. Dixit, Opt. Mater. 27 (2004) 261–264.
[34] T.D. Dzhafarov, F. Ongul, I. Karabay, J. Phys. D: Appl. Phys. 39 (2006) 3221–3225.
[35] I. Akyuz, S. Kose, F. Atay, V. Bilgin, Mater. Sci. Semicond. Process 10 (2007) 103–111.
[36] S.D. Chavhan, S. Senthilarasu, S.H. Lee, Appl. Surf. Sci. 254 (2008) 4539–4545.
[37] M.A. Rafea, A.A.M. Farag, N. Roushdy, J. Alloy. Compd. 485 (2009) 660–666.
[38] Y. Raviprakash, K.V. Bangera, G.K. Shivakumar, Curr. Appl. Phys. 10 (2010) 193–198.
[39] S. Li, Y. Jiang, M. Niu, C. Wang, J. Jie, J. Alloy. Compd. 481 (2009) 644–648.
[40] B.E. Warren, X-Ray Diffraction, Addison-Wesley, Reading, MA, 1969.
[41] J. Tauc, Amorphous and Liquid Semiconductor, Plenum Press, New York, 1974, p. 159.